Journal of Power Sources 245 (2014) 245–255

Contents lists available at SciVerse ScienceDirect

Journal of Power Sources

journal homepage: www.elsevier.com/locate/jpowsour

Composite cathode $La_{0.4}Sr_{0.4}TiO_{3-\delta}$–$Ce_{0.8}Sm_{0.2}O_{2-\delta}$ impregnated with Ni for high-temperature steam electrolysis

Yun Gan [a], Qingqing Qin [a], Shigang Chen [a], Yan Wang [a,b], Dehua Dong [c], Kui Xie [a,b,*], Yucheng Wu [a,b,*]

[a] Department of Energy Materials, School of Materials Science and Engineering, Hefei University of Technology, No. 193 Tunxi Road, Hefei, Anhui 230009, China
[b] Key Laboratory of Advanced Functional Materials and Devices, School of Materials Science and Engineering, Hefei University of Technology, No. 193 Tunxi Road, Hefei, Anhui 230009, China
[c] Fuels and Energy Technology Institute, Curtin University of Technology, 1 Turner Avenue, Technology Park, WA 6102, GPO Box U1987, Perth, WA 6845, Australia

HIGHLIGHTS

- Ni-loaded LSTO is utilized for direct steam electrolysis to produce hydrogen.
- Ni catalyst significantly improves the Faraday efficiency for steam electrolysis.
- The stability of Ni-loaded composite cathode is achieved for direct electrolysis.

ARTICLE INFO

Article history:
Received 25 March 2013
Received in revised form
18 June 2013
Accepted 18 June 2013
Available online 27 June 2013

Keywords:
Steam electrolysis
Solid oxide electrolyzer
Nickel
Strontium titanate

ABSTRACT

Composite Ni–SDC (Samaria doped Ceria) cathodes are able to operate in strong reducing atmospheres for steam electrolysis, and composite cathodes based on redox-stable $La_{0.4}Sr_{0.4}TiO_3$ (LSTO) have demonstrated promising performances without the reducing gas flow. However, the electro-catalytic activity of cathodes based on LSTO is insufficient for the efficient electrochemical reduction of steam or carbon oxide. In this work, catalytic-active Ni nanoparticles were loaded on a $La_{0.4}Sr_{0.4}TiO_{3-\delta}$–$Ce_{0.8}Sm_{0.2}O_{2-\delta}$ cathode (Ni-loaded LSTO–SDC) via an impregnation method to improve the electrode performances for direct steam electrolysis. The synergetic effect of catalytically-active Ni nanoparticles and the redox-stable LSTO–SDC skeleton contributed to the improved performances and the excellent stability of the cathode for direct steam electrolysis. The current efficiency with a Ni-loaded cathode was enhanced by 3% and 17% compared to the values with a bare LSTO–SDC cathode under 2.0 V of applied voltage at 800 °C with a flow of 3% H_2O/5% H_2/Ar and 3% H_2O/Ar to cathodes, respectively.

1. Introduction

Because the global climate change and correlated environmental problems are caused by fossil fuel combustion, many studies have focused on finding clean and renewable energy resources. Hydrogen is attracting growing interest and is considered the leading fuel candidate of the future because of its many advantages. For example, hydrogen is environmentally-friendly and can be produced from water using renewable electricity [1–5]. Solid oxide electrolyzers (SOEs) can efficiently produce hydrogen through high-temperature steam electrolysis, which directly converts electrical energy into chemical energy. Using external electricity, an oxide-ion-conducting solid oxide electrolyzer is able to electrolyze steam into hydrogen and oxygen. At the cathode, H_2O molecules are electrochemically reduced to H_2 under applied potential. The O^{2-} ions are transported through the oxide-ion conducting electrolyte membrane to the oxygen electrode compartment, where O_2 gas is formed and released [7–16].

Conventional Ni–YSZ has been preferentially used as a composite cathode in oxide-ion-conducting solid oxide electrolyzer for high-temperature steam electrolysis with the flow of reducing gas over the cathode in most reports [6,17–21]. However, the pre-reduction of the cathode and a significant concentration of

* Corresponding authors. Department of Energy Materials, School of Materials Science and Engineering, Hefei University of Technology, No. 193 Tunxi Road, Hefei, Anhui 230009, China.
E-mail addresses: xiekui@hfut.edu.cn (K. Xie), ycwu@hfut.edu.cn (Y. Wu).

0378-7753/$ – see front matter © 2013 Elsevier B.V. All rights reserved.
http://dx.doi.org/10.1016/j.jpowsour.2013.06.107

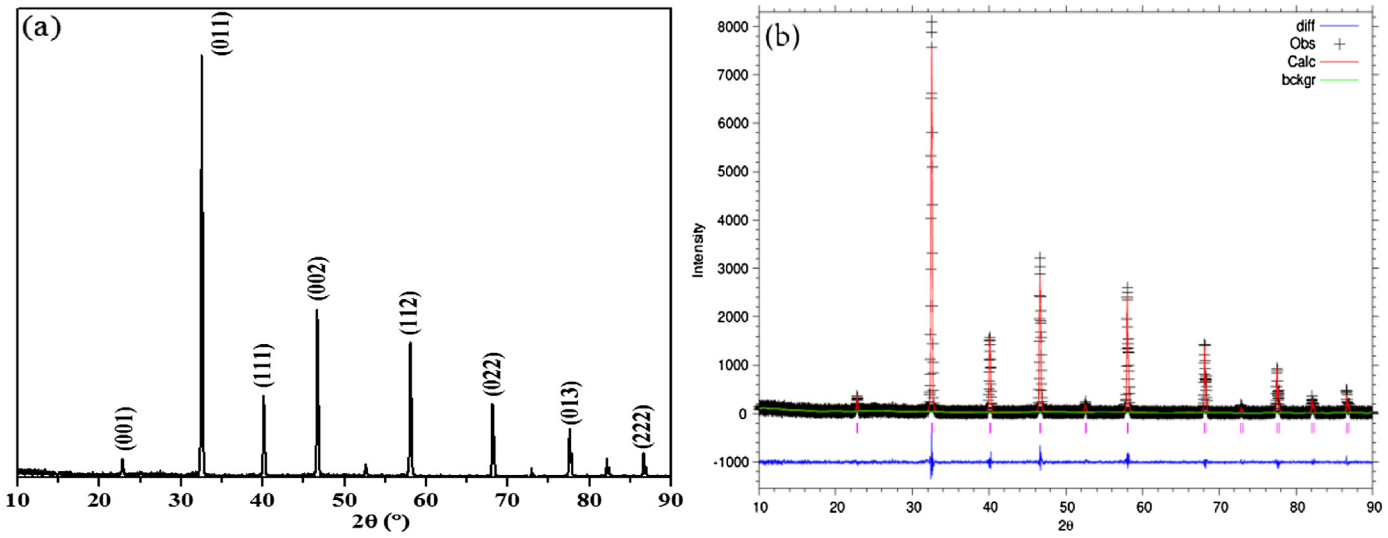

Fig. 1. (a) The XRD pattern of $La_{0.4}Sr_{0.4}TiO_{3-\delta}$ (LSTO) powder; (b) the Rietveld refinement of $La_{0.4}Sr_{0.4}TiO_{3-\delta}$ (LSTO) powder.

hydrogen in the cathode are required to prevent the Ni metal from being oxidized to NiO.

Perovskite-type $(La_{0.75}Sr_{0.25})_{0.95}Cr_{0.5}Mn_{0.5}O_3$ (LSCM) has been confirmed as an active and redox-stable electrode material that can be used both as a cathode and anode in solid oxide fuel cells [22,23]. Irvine et al. have recently demonstrated the feasibility of direct steam electrolysis using an LSCM–SDC cathode without the flow of reducing gas over the electrode in an oxide-ion-conducting solid oxide electrolyzer [10,24]; however, the steam electrolysis performance is still restricted by the insufficient catalytic activity of LSCM ceramics. We have recently discovered that some adverse chemical changes may occur in LSCM cathodes under strong reducing potential when performing high-temperature electrolysis, which further degrades the Faradic current efficiency as well as electrode performances [25]. On the other hand, the p-type conduction in LSCM is restricted when high voltage is applied to the cathode for electrochemical reduction of steam [8,26,27]. The perovskite, $La_xSr_{1-x}TiO_{3+\delta}$ (LSTO), is an active, redox-stable material, and it has high n-type conductivity upon reduction [16,24,28,29], which was demonstrated to be an alternative electrode material for direct steam electrolysis in our previous work [28]. In addition, the A-site deficiency in $La_xSr_{1-x}TiO_{3+\delta}$, e.g., $La_{0.4}Sr_{0.4}TiO_3$, results in an increased electronic conductivity of $La_xSr_{1-x}TiO_{3+\delta}$ under reducing conditions [30]. The reducing potential in the cathode can electrochemically reduce $La_xSr_{1-x}TiO_{3+\delta}$ and enhance the n-type conduction, which is expected to improve the electrode performance. However, similar problems, including insufficient catalytic activity, still exist for such types of ceramic cathodes, which hinder the enhancement of the performance of steam electrolysis.

In this work, catalytically-active Ni nanoparticles were loaded onto an LSTO–SDC composite cathode to enhance the electrocatalytic activity for steam electrolysis in an oxide-ion-conducting solid oxide electrolyzer. The electrical properties of LSTO were investigated and correlated to electrode performances. The use of Ni-loaded LSTO–SDC for steam electrolysis was systematically investigated at 800 °C with 3% H_2O/5% H_2/Ar and 3% H_2O/Ar fed into cathodes.

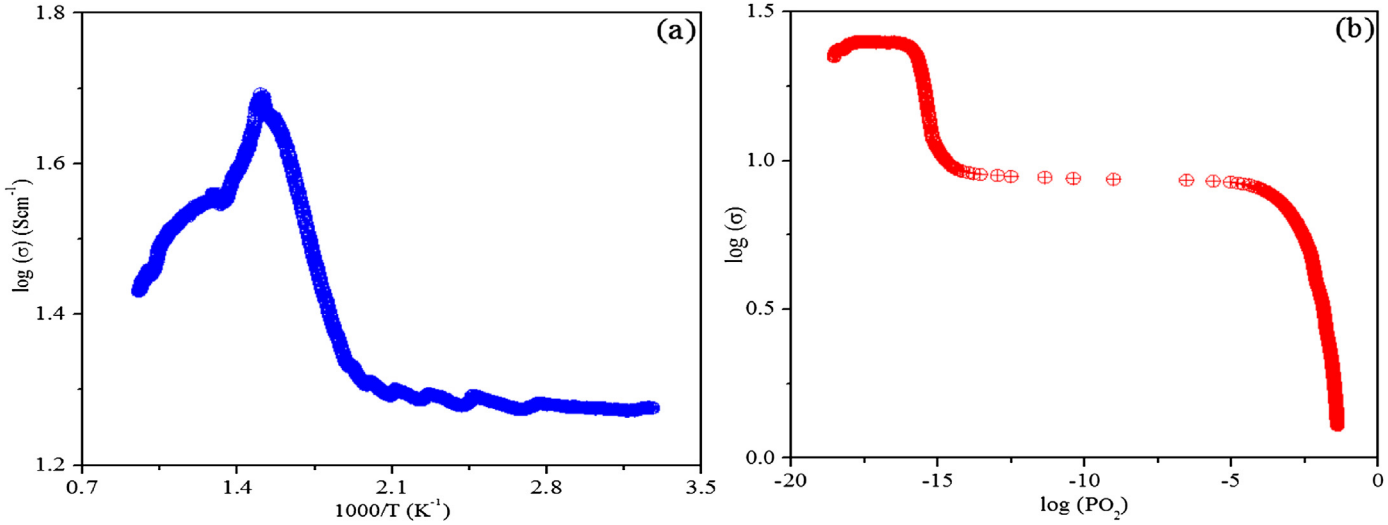

Fig. 2. The dependence of conductivity of $La_{0.4}Sr_{0.4}TiO_{3-\delta}$ (LSTO) on (a) temperature in 5% H_2/Ar and (b) the dependence of conductivity of LSTO on oxygen partial pressure at 800 °C.

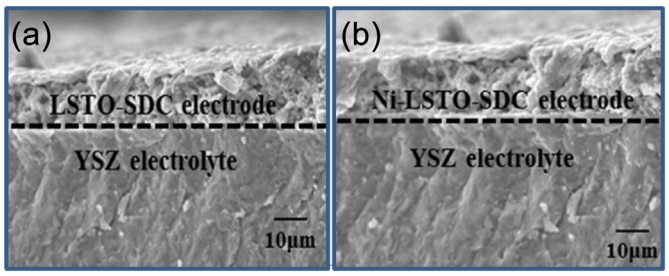

Fig. 3. The microstructures of symmetric solid oxide electrolyzers with of (a) LSTO–SDC/YSZ/LSTO–SDC and (b) Ni-LSTO–SDC/YSZ/Ni-LSTO–SDC configurations.

2. Experimental

$La_{0.4}Sr_{0.4}TiO_{3-\delta}$ (LSTO) powders were synthesized by a traditional solid-state reaction method [30–32]. Stoichiometric amounts of La_2O_3, $SrCO_3$, and TiO_2 were mixed in acetone and ground in a zirconia ball mills for 5 min. The dried powders were pressed into pellets and sintered at 1400 °C for 10 h in air. These pellets were then ground, and yellowish powders were obtained. $Ce_{0.8}Sm_{0.2}O_{2-\delta}$ (SDC) powders were prepared by a combustion method using Sm_2O_3 and $Ce(NO_3)_4{\cdot}6H_2O$ followed by a heat treatment at 800 °C for 3 h in air [33]. $(La_{0.8}Sr_{0.2})_{0.95}MnO_{3-\delta}$ powders were prepared in the same manner with the final heat treatment conducted at 1100 °C for 3 h in air. All these powders were bought from SINOPHARM Chemical Reagent Co. Ltd (China). The phase formation of the LSTO, SDC and LSM powders was analyzed by X-ray diffraction (XRD, $2\theta = 3°$ min^{-1}, D/MAX2500 V, Rigaku Corporation, Japan).

Approximately 2.5 g of LSTO powder was pressed into a bar and then sintered at 1400 °C for 10 h in air, and the relative density reached 82.3%. Subsequently, the samples were reduced at 1100 °C for 24 h in 5% H_2/Ar. The conductivity tests in reducing atmosphere were performed using a DC four-terminal method from 30 °C to 800 °C in 5% H_2/Ar. The conductivity was recorded with an online system with a step of 0.5 °C. The dependence of conductivity on the partial oxygen pressure (PO_2) was recorded with the PO_2 ranging from 10^{-20} to 0.05 atm. At first, the flow rate of 5% H_2/Ar was

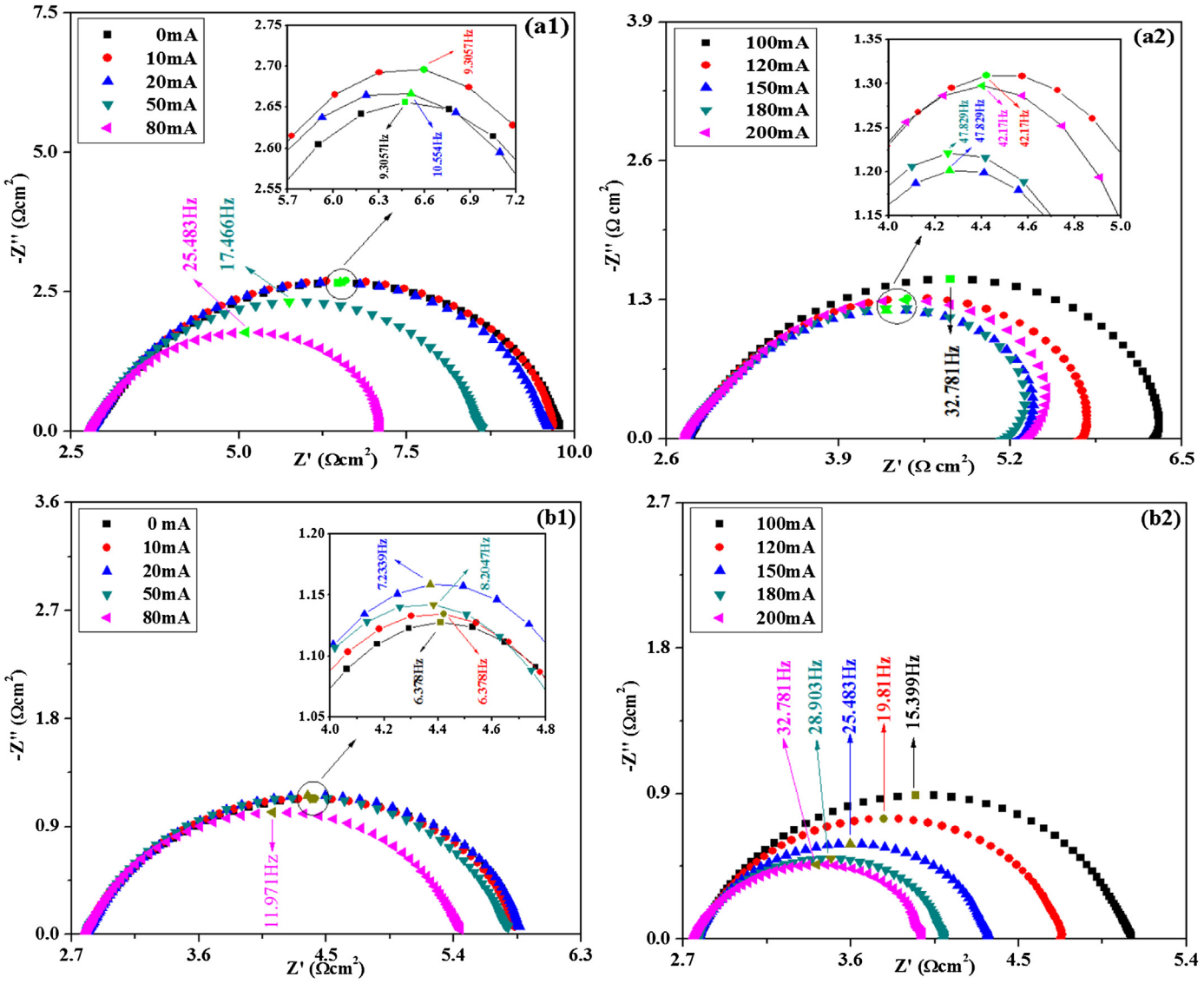

Fig. 4. In-situ AC impedance of symmetric solid oxide electrolyzers with cathodes based on (a1) (a2) LSTO–SDC and (b1) (b2) Ni-LSTO–SDC under different applied currents in a 5% H_2/Ar atmosphere.

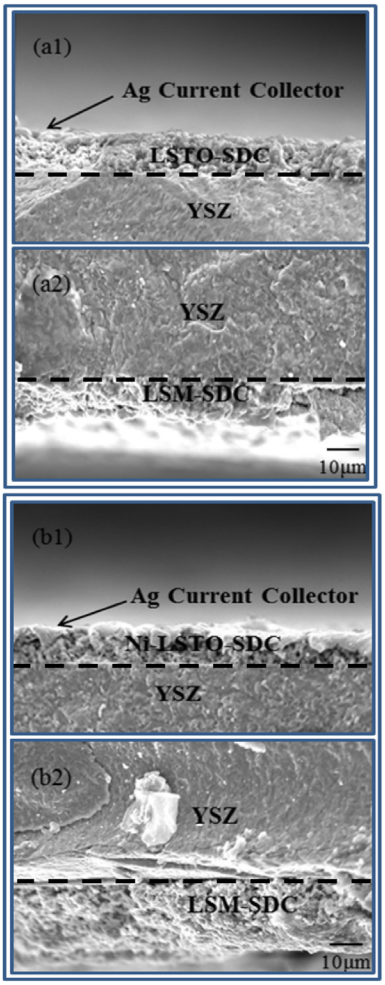

Fig. 5. The microstructures of the electrolyzers with configurations of (a1, a2) LSTO–SDC/YSZ/LSM–SDC and (b1, b2) Ni-LSTO–SDC/YSZ/LSM–SDC.

controlled at 60 ml min^{-1} throughout the test to maintain the PO_2 at 10^{-20} atm. Then the air flow was controlled at a rate of 0.5 ml min^{-1} to change the PO_2 after terminating the input of 5% H_2/Ar. The PO_2 and the conductivity were simultaneously recorded with an online oxygen sensor (Type 1231, ZrO_2-based oxygen sensor, Noveltech, Australia) and an online multi-meter (Keithley 2000, Digital Multimeter, Keithley Instruments Inc., USA), respectively, and the total gas pressure was controlled at 1.0 atm.

The 8YSZ powder was dry-pressed into a green disk with a diameter of 20 mm followed by a sintering in air at 1500 °C (3 °C min^{-1}) for 10 h to prepare 2-mm-thick 8YSZ electrolyte supports. Then, two surfaces of the electrolyte supports were mechanically polished and ultrasonically cleaned in ethanol and distilled water. LSTO–SDC slurries were prepared by milling the LSTO and SDC powders (at a ratio 65:35), followed by grounding in alpha-terpineol with appropriate amounts of cellulose additives. The composite LSM–SDC slurries were prepared by milling SDC powder with LSM powder at a weight ratio of 35:65 in the alpha-terpineol with the cellulose additive in a similar manner. The electrodes were then coated onto the electrolyte over an area of 1.0 cm^2 and treated at 1100 °C (3 °C min^{-1}) for 3 h in air. $Ni(NO_3)_2$ solution was then impregnated into an LSTO–SDC electrode to create Ni-loaded composite cathodes [34]. Silver paste (SS-8060, Xinyi, Shanghai, China) was printed onto both electrode surfaces for current collecting. A scanning electron microscope (SEM, JSM-6490LV, JEOL Ltd, Japan) was used to observe the microstructures of the as-prepared electrolyzers. An external circuit was made with silver wire (0.4 mm in diameter), which was fastened to current collectors using silver paste (DAD87, Shanghai Research Institute for Synthetic Resins, Shanghai, China) and then heated at 550 °C (3 °C min^{-1}) for 30 min in air. The single solid oxide electrolyzers were prepared by coating LSM–SDC on one side, whereas Ni-loaded LSTO–SDC and bare LSTO–SDC slurries were coated on the other side. Symmetric solid oxide electrolyzers with LSTO–SDC and Ni-loaded LSTO–SDC were prepared in the same way.

Initially, AC impedance of the symmetric solid oxide electrolyzers tested in 5% H_2/Ar with different applied current at 800 °C was conducted using an electrochemical workstation (IM6, Zahner, Germany). The electrode polarization resistance was calculated by modeling the spectra using Zview software. The gas flow rate was controlled at 20 ml min^{-1} using a mass flow meter (D08-3F,

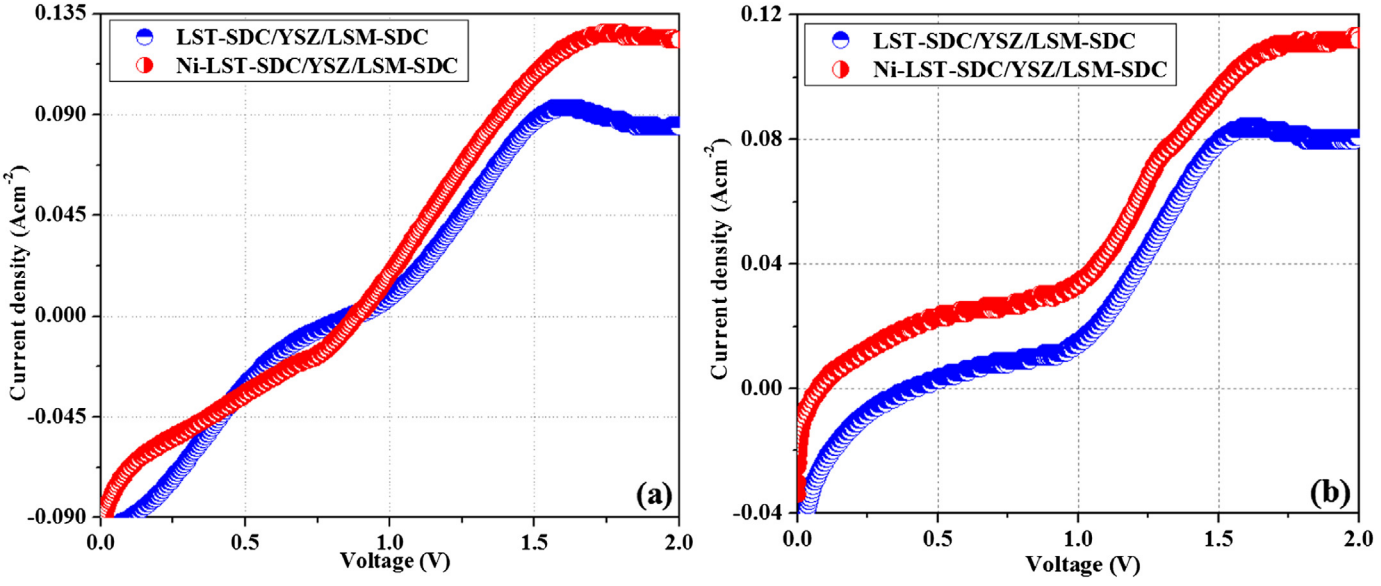

Fig. 6. The *I–V* curve of two types of single solid oxide electrolyzers tested (a) with a flow of 3% H_2O/5% H_2/Ar and (b) 3% H_2O/Ar.

Sevenstar, Beijing, China). Then, the single solid oxide electrolyzers were sealed to a home-made testing jig by using ceramic paste (JD-767, Jiudian, Dongguan, China) for electrochemical measurements, including the AC impedance and Current–Voltage (I–V) curve. Direct steam electrolysis was performed at 1.0, 1.2, 1.4, 1.6, 1.8 and 2.0 V with the as-prepared single solid oxide electrolyzers at 800 °C in 3% H_2O/5% H_2/Ar and 3% H_2O/Ar. The output gas from the cathode was analyzed using an online gas chromatograph (GC9790II, Fuli, Zhejiang, China), with an aim of detecting the concentration of generated hydrogen. The long-term performance of solid oxide electrolyzer based on Ni-loaded LSTO–SDC was evaluated at a fixed voltage at 800 °C to observe the stability of the detected current densities. SEM, XRD and EDX were utilized to analyze the cathodes before and after steam electrolysis test.

3. Results and discussion

Fig. 1(a) shows the XRD patterns of the LSTO prepared by a traditional solid-state reaction method at 1400 °C for 10 h in air. All the samples displayed pure phase according to the references [30–32], and the XRD pattern was indexed according to the PDF card (No. 52-1769). The patterns of LSTO powders were refined using GSAS software as shown in Fig. 1(b). In our work, the LSTO is $La_{0.4}Sr_{0.4}TiO_3$, and the reference is $La_{0.4}Sr_{0.6}TiO_{3+\delta}$ (Pm-3m, $a = b = c = 3.9081$ nm, $\alpha = \beta = \gamma = 90°$). These two oxides belong to the same space group; however, the chemical compositions are different. The refinement gives χ^2, wRp and Rp values of 6.106, 0.2573 and 0.1668, respectively, and the cell parameters of LSTO are $a = b = c = 3.8876$ nm and $\alpha = \beta = \gamma = 90°$.

As shown in Fig. 2(a), the conductivity of the reduced LSTO sample displayed typical metallic behavior in the 5% H_2/Ar atmosphere because of the n-type conducting mechanism. The reduced LSTO is an n-type electronic conductor; however, as shown in Fig. 2(a), the temperature dependence of conductivity displayed a semiconducting behavior with a positive temperature coefficient up to 391 °C. The adsorption of oxygen oxidized the Ti^{3+} to Ti^{4+} on the surface of the reduced LSTO, which produced an oxidized and p-type conducting LSTO layer on the surface and

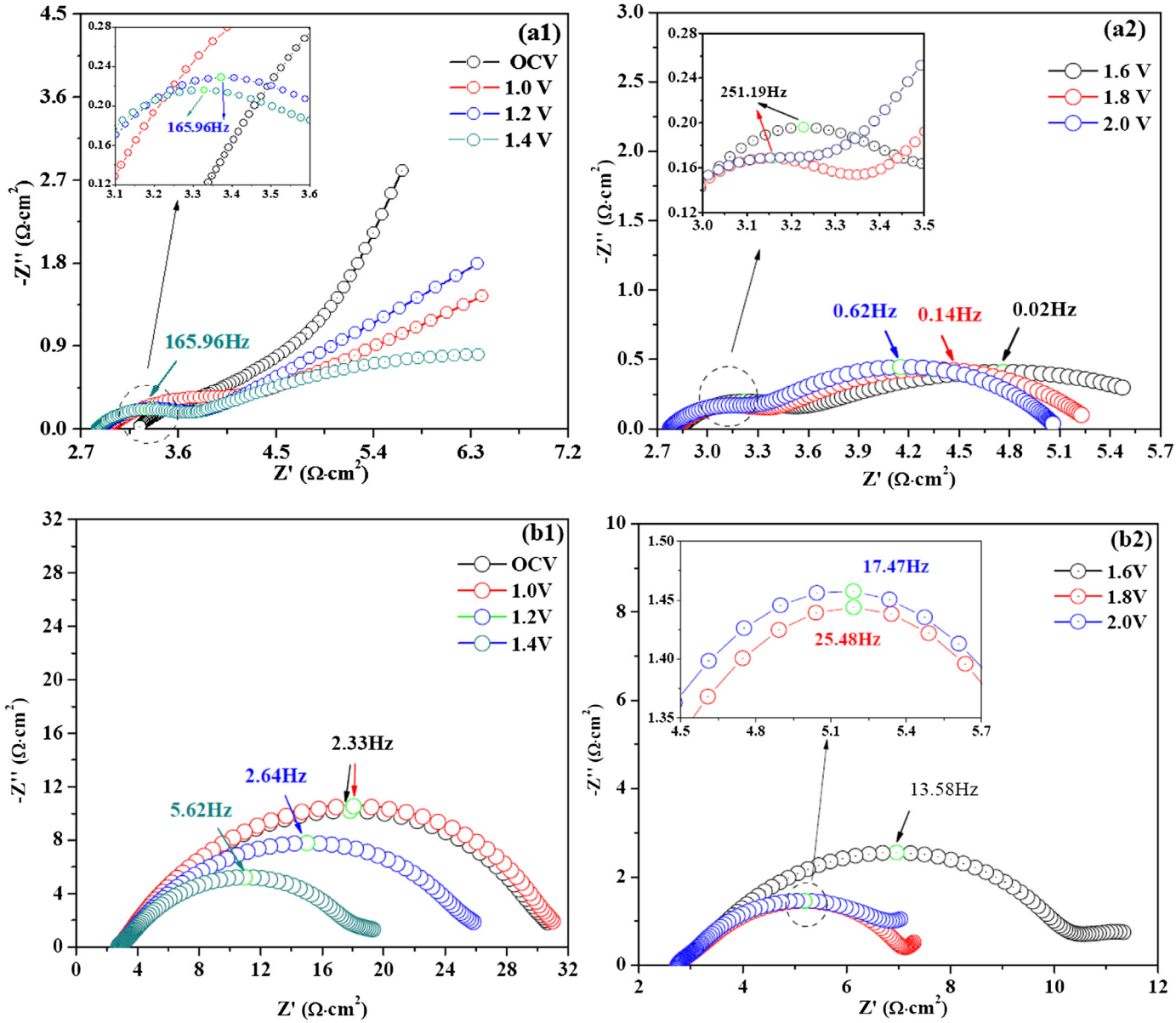

Fig. 7. In-situ AC impedance of a single electrolyzer with cathodes based on (a1, a2) Ni-LSTO–SDC and (b1, b2) LSTO–SDC at different voltages in 3% H_2O/5% H_2/Ar.

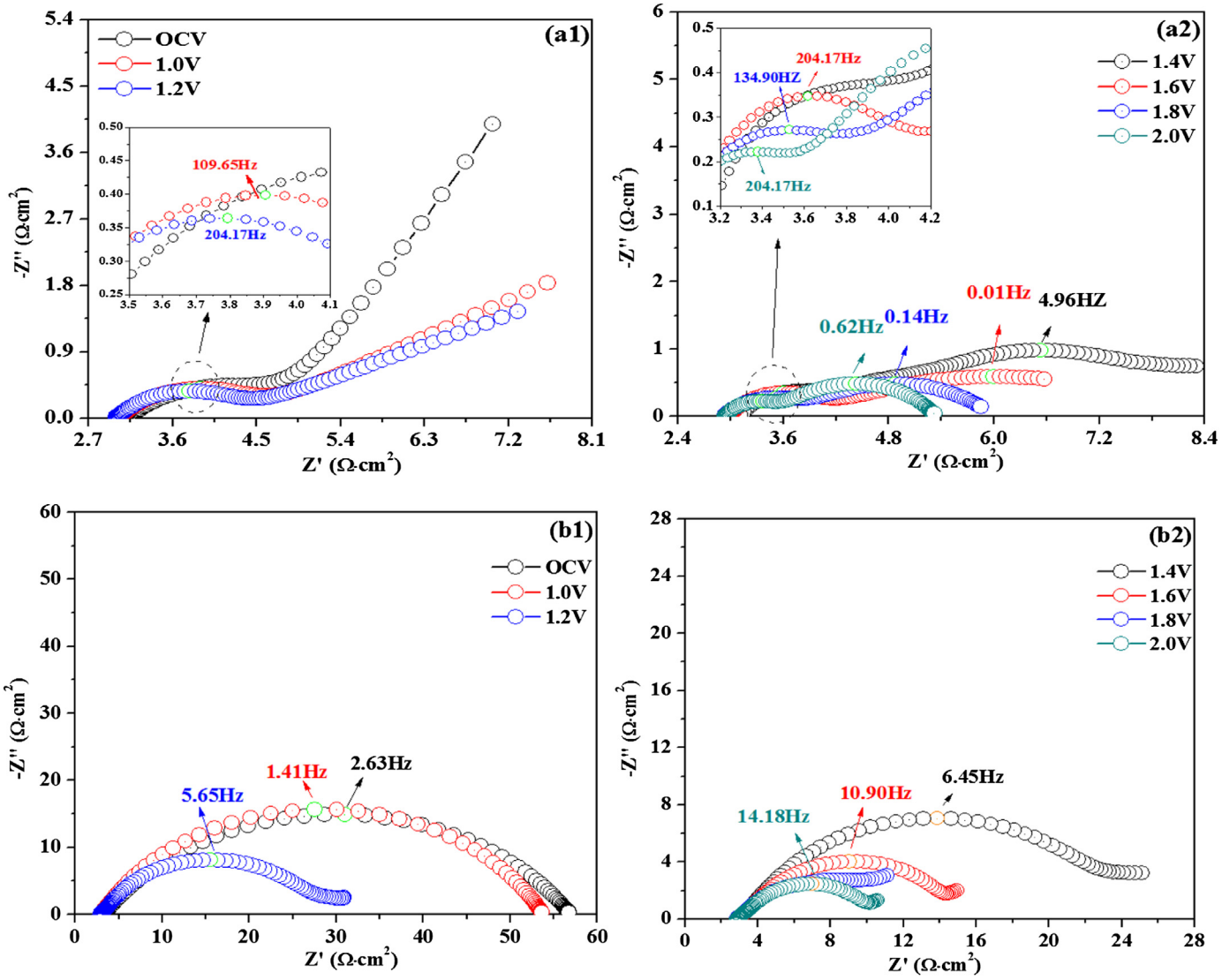

Fig. 8. In-situ AC impedance of a single electrolyzer with cathodes based on (a1, a2) Ni-LSTO–SDC and (b1, b2) LSTO–SDC at different applied voltages in 3% H_2O/Ar.

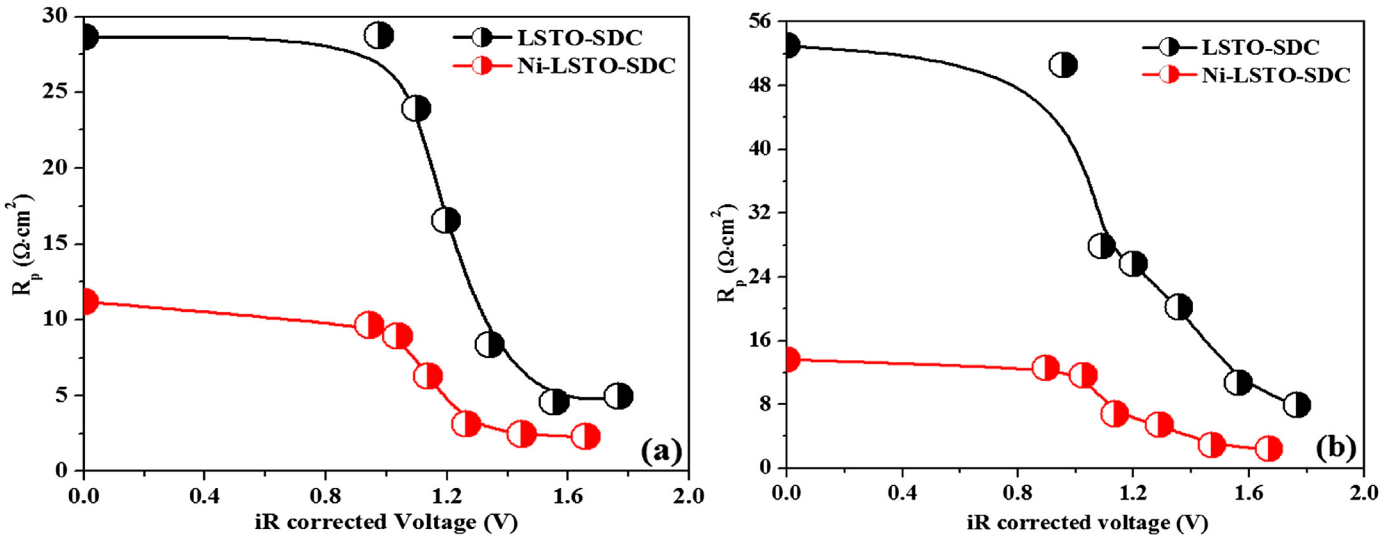

Fig. 9. R_p versus i.R corrected voltage of the electrolyzer tested in (a) 3% H_2O/5% H_2/Ar and (b) 3% H_2O/Ar at 800 °C.

caused the low conductivity of reduced LSTO at low temperatures [35]. However, the hydrogen atmosphere gradually and sufficiently reduced the adsorbed oxygen up to 391 °C, which greatly improved the electrical conductivity though the n-type conductivity dropped with temperature. The conductivity of the reduced LSTO reached approximately 49 S cm^{-1} at 391 °C; however, a negative temperature coefficient was observed between 391 and 800 °C. This was typical metallic behavior in wet hydrogen, and the conductivity finally decreased to approximately 27 S cm^{-1}. The conductivity of the reduced LSTO sample was strongly dependent on the partial oxygen pressure (PO_2) as shown in Fig. 2(b). The conductivity of the LSTO sample was remarkably increased at low PO_2 because of the increase of the charge carrier concentration in the stronger reducing atmosphere, which further confirms the n-type conduction of the reduced LSTO material.

Fig. 3(a) and (b) shows the microstructures of the symmetric cells with configurations of LSTO–SDC/YSZ/LSTO–SDC and Ni-LSTO–SDC/YSZ/Ni-LSTO–SDC, respectively. The adhesion appeared to be very strong between the dense electrolyte and the 10-μm-thick porous electrode layers. Fig. 4 shows the *in-situ* AC impedance of the symmetric cells tested in 5% H_2/Ar at 800 °C under a series of applied current densities. There are two intercepts with the real axis in the impedance spectra, and the first intercept at high frequency corresponds to the series resistance (R_s) of the cell, which mainly results from the ionic resistance of the YSZ electrolyte [36]. The difference between the two intercepts is regarded as the electrode polarization resistance (R_p). As shown in Fig. 4(a1) and (a2), the R_p is 3.65 Ω cm^2 when no current is applied; however, it dramatically drops to 1.25 Ω cm^2 when the applied current density reaches 200 mA cm^{-2}, which implies that the ceramic electrode could be activated when the current density passed through the two electrodes. Though the reduction and oxidation reactions take place at two electrodes, the improved electrode polarizations still demonstrated the enhanced electro-catalytic activity when the current density passed through both electrodes. In contrast, a more significant improvement of the R_p of the symmetric cell was observed with the Ni-loaded LSTO–SDC composite electrode as shown in Fig. 4(b1) and (b2). The R_p is only 1.55 Ω cm^2 at 0 mA cm^{-2} and further drops to 0.65 Ω cm^2 at 200 mA cm^{-2}, which indicates that the catalytic-active Ni particles greatly enhance the electro-catalytic properties of the composite electrodes and accordingly reduce the electrode polarization resistances of the symmetric cell. The improved performance of Ni-loaded LSTO–SDC electrode further benefits the electrochemical process of steam electrolysis and simultaneously enhances the Faradic efficiency.

Fig. 5(a) and (b) shows the microstructures of the single solid oxide electrolyzer with a LSTO–SDC/YSZ/LSM–SDC configuration, whereas Fig. 5(c) and (d) shows the microstructures of the single solid oxide electrolyzer with a Ni-LSTO–SDC/YSZ/LSM–SDC configuration. The adhesion appears strong between the dense YSZ

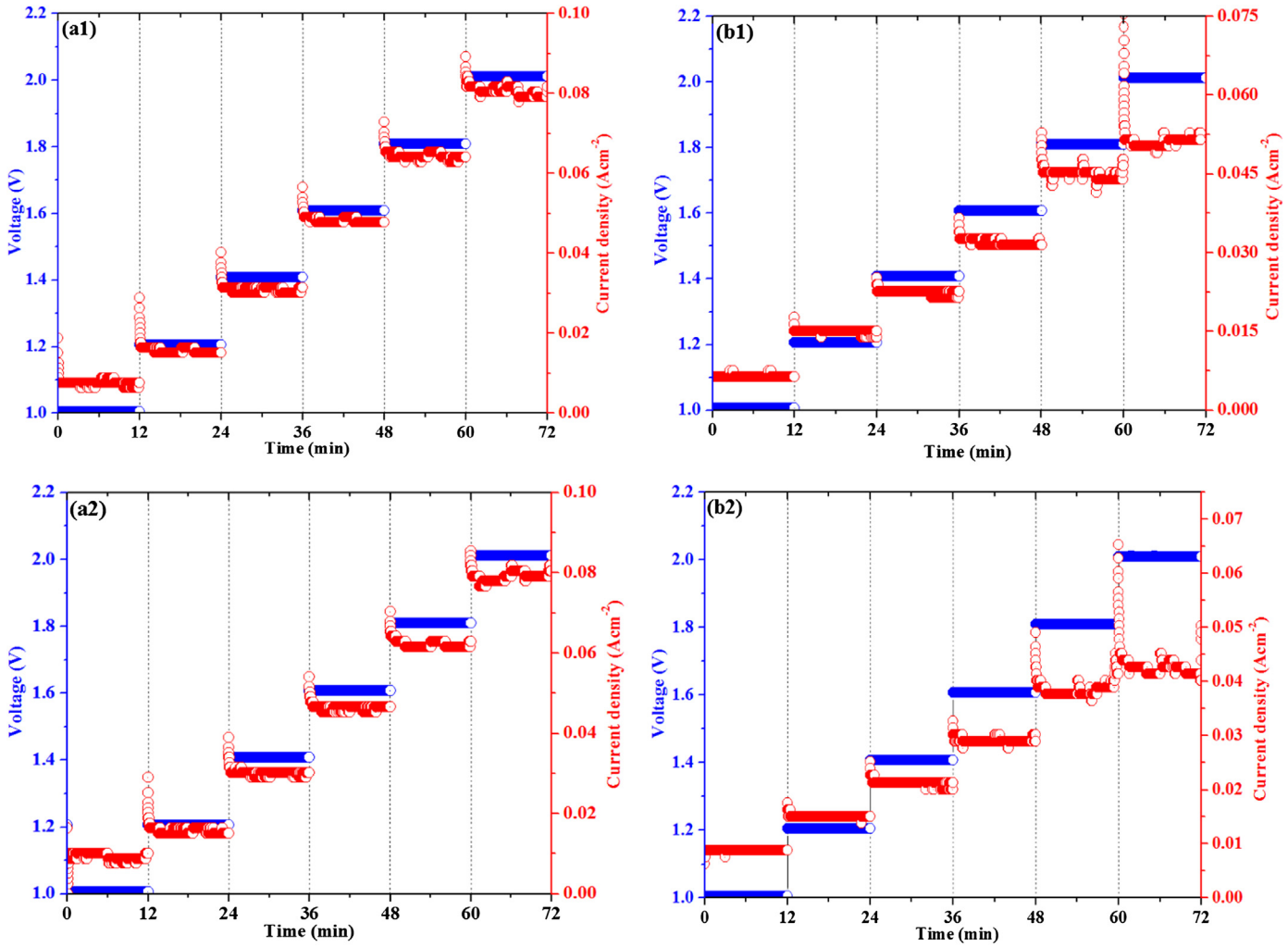

Fig. 10. The short-term steam electrolysis performance with (a1) Ni-LSTO–SDC and 3% H_2O/5% H_2/Ar; (b1) LSTO–SDC and 3% H_2O/5% H_2/Ar; (a2) Ni-LSTO–SDC and 3% H_2O/Ar; (b2) LSTO–SDC and 3% H_2O/Ar.

electrolytes with tiny porosities and the porous 12-μm-thick electrode layers. Steam electrolysis was performed in both solid oxide electrolyzers at 800 °C with 3% H_2O/5% H_2/Ar and 3% H_2O/Ar fed into the cathodes, respectively. Fig. 6 shows the current density with the applied voltage (*I–V* curve) of the two types of electrolyzers under different testing conditions. The open circuit voltages of the single electrolyzers in 3% H_2O/5% H_2/Ar are 0.9 V as shown in Fig. 6(a), which are consistent with but still a little lower than the OCV for a solid oxide fuel cell with H_2 fuel. The relationship between the current density and applied voltage are far from linear, and clear changes in slope can be observed above 1.2 V. The maximum current density reaches 0.123 A cm^{-2} at 2.0 V based on Ni-loaded LSTO–SDC composite cathodes, whereas the current density only reaches 0.085 A cm^{-2} with bare LSTO–SDC electrodes in 3% H_2O/5% H_2/Ar, which indicates that the loading of the Ni catalyst significantly enhances the cell performance for steam electrolysis. Similar behaviors were also observed for the electrolyzers in 3% H_2O/Ar as shown in Fig. 6(b), where the current density reached 0.112 A cm^{-2} at 2.0 V with Ni-loaded LSTO–SDC composite cathodes; however, only 0.080 A cm^{-2} was achieved with LSTO–SDC, which further confirms the improvement of electrode performance by loading a Ni catalyst on the cathodes even in a less reducing atmosphere, 3% H_2O/Ar. It should also be noted that the current densities based on Ni-loaded LSTO–SDC and LSTO–SDC in 3% H_2O/5% H_2/Ar are both slightly larger than those in 3% H_2O/Ar, which might be attributed to the better catalytic performances and mixed conductivities of the composite electrodes in more reducing conditions. To further study the electrochemical performance of the electrodes, *in-situ* AC impedance spectroscopy was conducted to investigate the change of cell resistance under different voltages.

Figs. 7 and 8 show the *in-situ* AC impendence of solid oxide electrolyzers under a series of external voltages ranging from 1.0 to 2.0 V, at 800 °C in 3% H_2O/5% H_2/Ar and 3% H_2O/Ar, respectively. As shown in the figures, the electrode polarization resistance R_p is quite large at low voltages, whereas the increasing voltages make the R_p drop considerably at high voltages, which may be attributed to the fact that the applied voltage not only activates the electrode but also electrochemically reduces the composite LSTO–SDC electrode and enhances the mixed conductivity [24,28]. The R_p is only 2.58 Ω cm^2 at 1.6 V and further drops to 2.28 Ω cm^2 at 2.0 V in 3% H_2O/5% H_2/Ar with Ni-loaded LSTO–SDC cathode, whereas the R_p is approximately 8.54 Ω cm^2 at 1.6 V but still reaches 4.94 Ω cm^2 at 2.0 V with the LSTO–SDC cathode as shown in Fig. 7(a) and (b). These results further indicate that the Ni catalyst enhanced the electro-catalytic activity of the composite electrodes and accordingly reduced the electrode polarization resistances. A promising electrochemical performance with the Ni-loaded LSTO–SDC composite cathodes was also obtained in the 3% H_2O/Ar atmosphere for direct steam electrolysis as shown in Fig. 8. Direct steam electrolysis was achieved with the Ni-loaded composite cathode, and a comparable

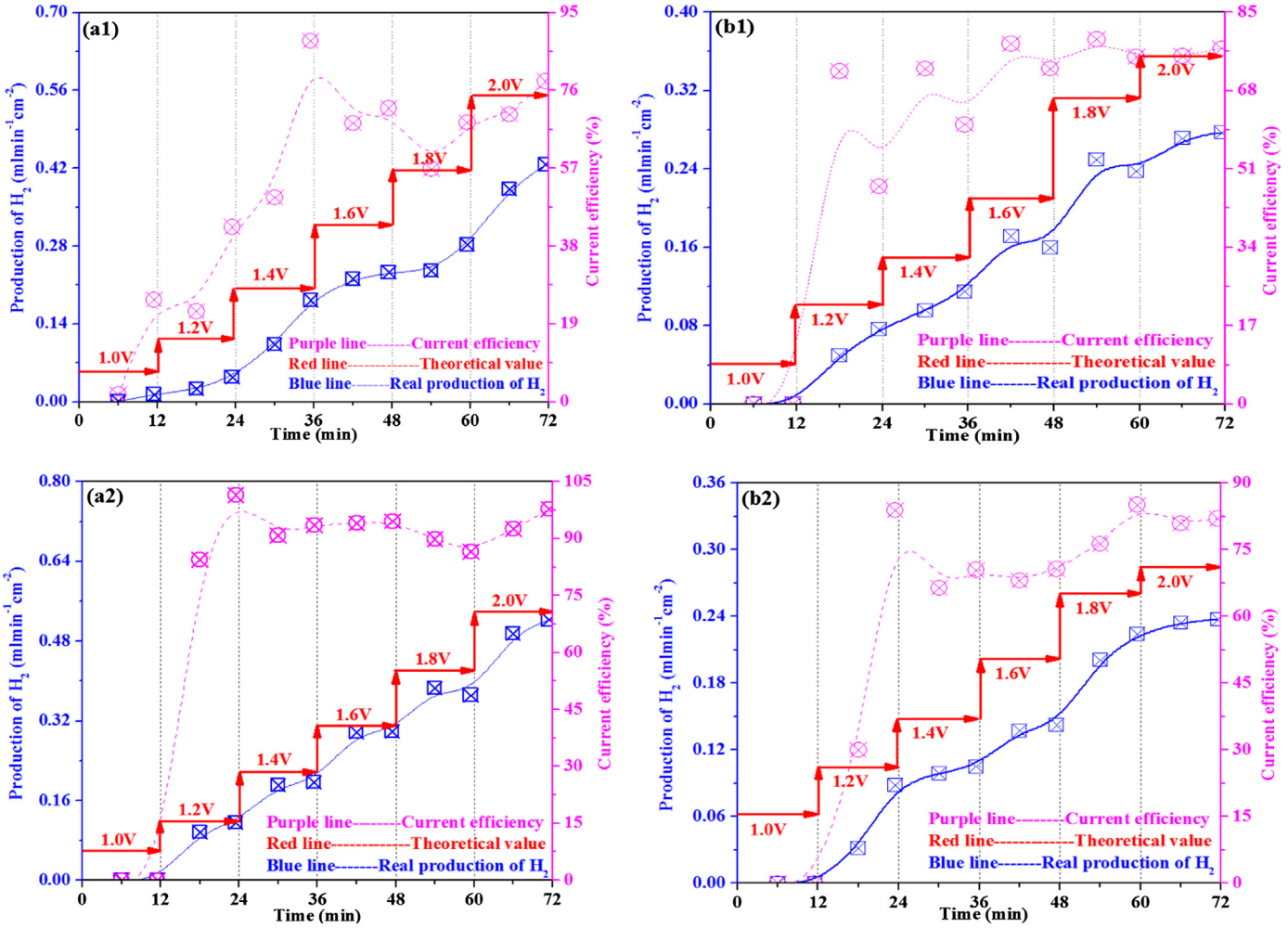

Fig. 11. The hydrogen production and current efficiency of the electrolyzer with (a1) Ni-LSTO–SDC and 3% H_2O/5% H_2/Ar; (b1) LSTO–SDC and 3% H_2O/5% H_2/Ar; (a2) Ni-LSTO–SDC and 3% H_2O/Ar; (b2) LSTO–SDC and 3% H_2O/Ar.

performance with electrolyzers in 3% H_2O/Ar was obtained. The electrode polarization resistance with the Ni-loaded LSTO–SDC cathode, R_p, is 2.91 Ω cm^2 at 1.8 V and finally drops to 2.39 Ω cm^2 at 2.0 V, which is comparable but slightly larger than the values in 3% H_2O/5% H_2/Ar. However, the R_p with the bare LSTO–SDC electrode is approximately 10.69 Ω cm^2 at 1.8 V and 7.67 Ω cm^2 at 2.0 V, which is most likely because the direct steam electrolysis produces a less reducing atmosphere that decreases the mixed conductivity of the LSTO–SDC composite electrodes. Therefore, it is reasonable to conclude that the composite electrode with the Ni catalyst demonstrated better performances than the bare LSTO–SDC electrode in both atmospheres, especially for direct steam electrolysis without a flow of reducing gas, 5% H_2/Ar, over the cathodes.

Fig. 9(a) and (b) shows the R_p versus i.R corrected voltages in different atmospheres. These data allow further understanding of the changes under different voltages where the voltages of i.R were subtracted. In Fig. 9(a), it is obvious that the R_p values from the electrode polarizations decrease significantly from 28.6 Ω cm^2 at an open circuit voltage to 4.94 Ω cm^2 at 2.0 V with the bare LSTO–SDC electrode, whereas the R_p of the electrode based on the Ni-loaded LSTO–SDC displays a significant decrease from 11.2 Ω cm^2 at an open circuit voltage to 2.28 Ω cm^2 at 2.0 V. Similar results were obtained in a 3% H_2O/Ar atmosphere for both types of electrolyzers as shown in Fig. 9(b). The R_p value obtained from the gradients of the I–V curves at lower potentials are slightly higher than the values measured by the A.C. methods but display a consistent trend with the results from the D.C. measurements.

The current densities versus time with the applied voltage of 1.0, 1.2, 1.4, 1.6, 1.8 and 2.0 V were also recorded to further investigate the process of steam electrolysis (Fig. 10). It is clear that the current densities increased with the applied voltage and the performance was stable at a certain potential load. It can also be observed that

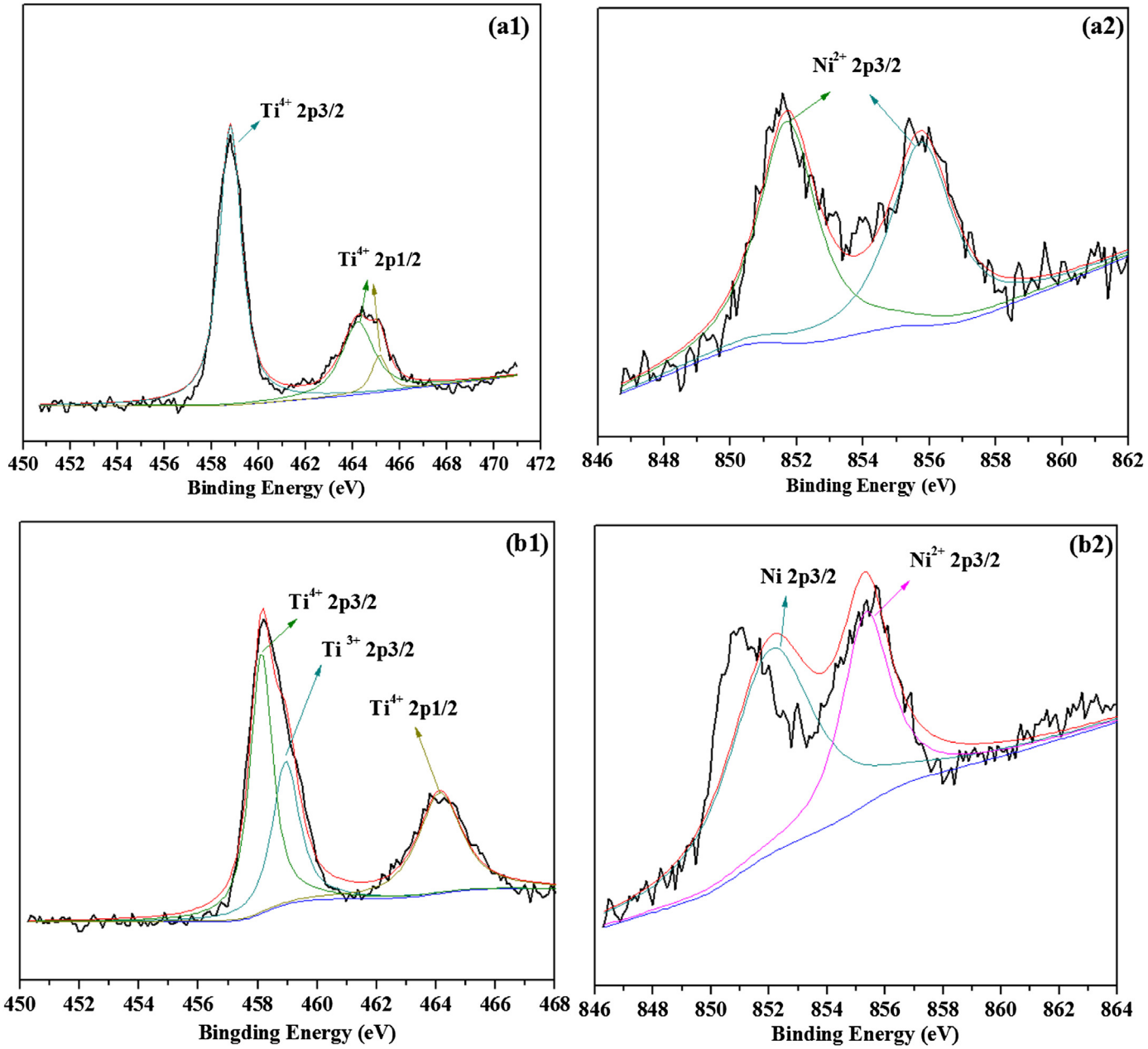

Fig. 12. XPS results for Ti (a1), Ni (a2) in oxided Ni-loaded $La_{0.4}Sr_{0.4}TiO_3$; Ti (b1), Ni (b2) in reduced Ni-loaded $La_{0.4}Sr_{0.4}TiO_{3-\delta}$.

the current density reached approximately 0.08 A cm^{-2} at 2.0 V with the Ni-loaded LSTO–SDC electrodes, which is higher than 0.05 A cm^{-2} for the bare LSTO–SDC electrodes in 3% H_2O/5% H_2/Ar. In addition, the current density with the Ni-loaded LSTO–SDC cathodes still reached a comparable 0.08 A cm^{-2} in 3% H_2O/Ar for direct steam electrolysis; however, the current density for the bare LSTO–SDC electrode in 3% H_2O/Ar dropped to 0.04 A cm^{-2}.

Fig. 11 shows the hydrogen production rate, and current efficiency with the Ni-loaded LSTO–SDC and bare LSTO–SDC cathodes under different applied voltages for steam electrolysis in 3% H_2O/5% H_2/Ar and 3% H_2O/Ar at 800 °C, respectively. There was no H_2 produced at 1.0 V, which is attributed to the fact that the OCV of a H_2-fed SOFC is above 1.0 V. The production of H_2 reached 0.278 ml min^{-1} cm^{-2} at 2.0 V with the bare LSTO–SDC composite electrode in 3% H_2O/5% H_2/Ar, whereas the Ni-loaded LSTO–SDC composite electrode demonstrated a H_2 production of 0.426 ml min^{-1} cm^{-2} under the same conditions. More importantly, direct steam electrolysis was achieved with the Ni-loaded LSTO–SDC composite cathodes in the 3% H_2O/Ar atmosphere without inputting the reducing gas to protect the Ni metal. The hydrogen generation from the direct electrolysis of 3% H_2O/Ar reaches 0.523 ml min^{-1} cm^{-2} for the Ni-loaded LSTO–SDC composite cathodes, which is slightly higher than the performance, 0.289 ml min^{-1} cm^{-2}, for the bare LSTO–SDC electrode. The hydrogen generated in the cathode from direct steam electrolysis protects the Ni metal from being oxidized, whereas the Ni catalyst simultaneously enhances the electro-catalytic activity of the composite electrode. These results suggest that the synergetic effect of the catalytically-active Ni and redox-stable LSTO–SDC leads to the improved cathode performances for direct steam electrolysis and desired short-term stability. The corresponding current efficiency reached 78.21% and 97.77% at 2.0 V with the Ni-loaded LSTO–SDC cathodes in 3% H_2O/5% H_2/Ar and 3% H_2O/Ar, whereas only 75.47% and 81.97% were obtained with the bare LSTO–SDC electrode in 3% H_2O/5% H_2/Ar and 3% H_2O/Ar. A significant improvement was observed in current efficiency of steam electrolysis when the Ni catalyst was loaded on the cathode, especially under the atmosphere without a flowing reducing gas in the cathodes. It should be noted that the enhancement of the Ni-loaded cathode performance is much better at low voltage (1.3–1.8 V), but the current efficiency with the modified cathodes is only approximately 5–10% higher than the bare cathode at high voltage, for example at 2.0 V. The similar performances at high voltage might be related to the low frequency process as presented in A.C. impedance, which reflects the mass transfer, adsorption, desorption and diffusion associated with the electrode microstructure. The microstructure engineering of the electrode will be studied in a future work as the adsorption and desorption of steam at high levels might be strongly dependent on the cathode microstructures and operation temperatures.

Fig. 12 shows the XPS results of the Ni and Ti elements in the oxidized and reduced samples. As shown in Fig. 12(a2), only Ti^{4+} is observed in the oxidized composite electrode. However, part of the Ti^{4+} is reduced to Ti^{3+} which is observed in the reduced electrode as shown in Fig. 12(b2). The impregnated Ni in the oxidized composite electrode is at the Ni^{2+} (NiO) oxidation state, whereas it exists in the form of metallic nickel particles in the reduced sample as shown in Fig. 12(a2) and (b2). These results confirm the existence of elemental Ni and the transformation of NiO to metallic Ni on the ceramic substrate. The appearance of the Ni^{2+} signal in the reduced sample is most likely related to the adsorption of atmospheric oxygen, which leads to the oxidation of Ni metal into NiO on the sample surface. Fig. 13(a) shows the XRD patterns of the Ni-loaded LSTO–SDC cathodes before and after the steam electrolysis test at 800 °C. The NiO phase was observed in the cathodes before the test; however, Ni metal transformed from NiO appeared after the test, which confirms the presence of catalytically-active Ni particles in the composite cathodes. SEM and EDX were used together to analyze the cathode. As shown in Fig. 13(b), the elemental Ni was homogeneously dispersed in the cathodes, which was expected to improve the electro-catalytic performances of the cathodes. To validate the stability of the Ni-loaded composite electrodes, direct steam electrolysis was performed at a fixed voltage of 1.6 V for 22 h. As shown in Fig. 14(a), the current density decreases approximately 15% in the first 8 h; however, it appears to a stable level after running for a longer time. The degradation of the cell performance at the beginning might be due to agglomeration of Ni nanoparticles but the short-term performance of the Ni-loaded composite cathode was generally stable. SEM and EDX were used to analyze the cathode to characterize the microstructure evolution after the short-term test. Slight agglomeration of nickel nanoparticles was observed from the nickel-element mapping as

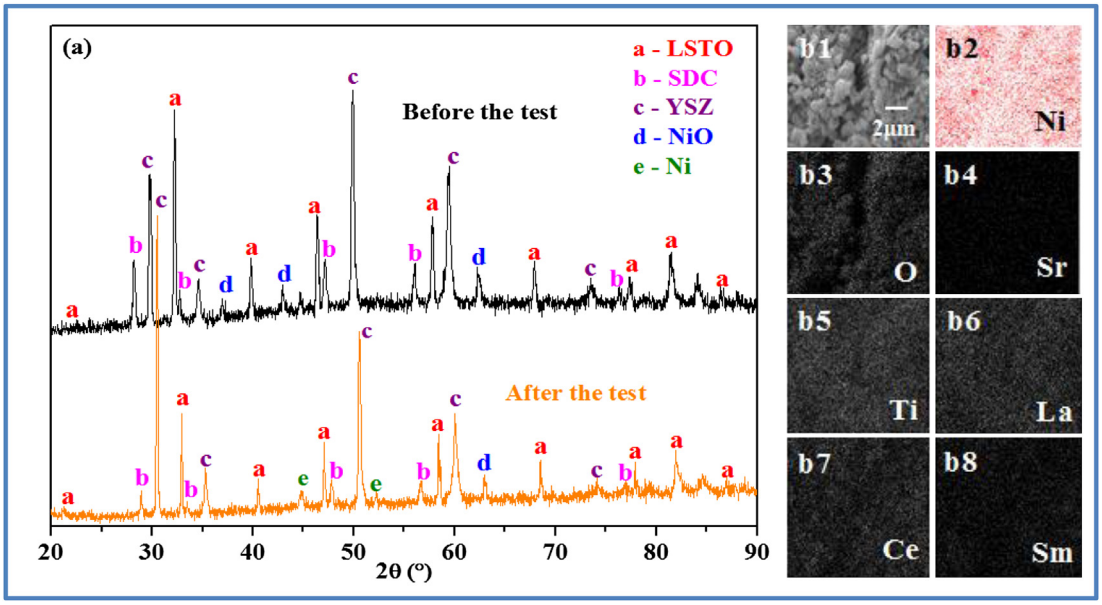

Fig. 13. XRD, SEM and EDX of Ni-loaded LSTO/SDC cathodes before and after the test for steam electrolysis at 800 °C.

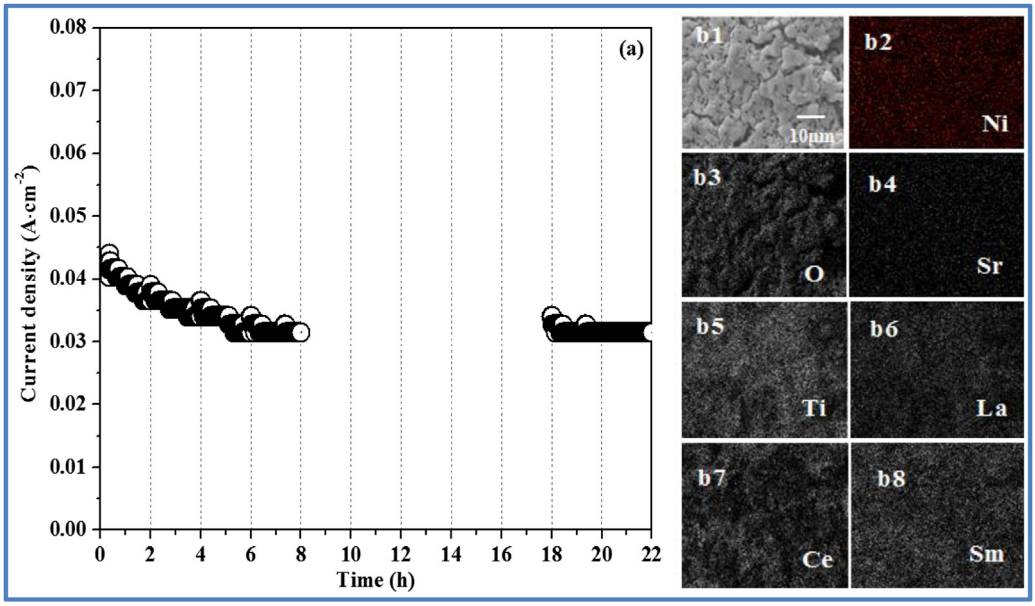

Fig. 14. (a) Short-term performance of the Ni-loaded LSTO–SDC for 3% H_2O/Ar steam electrolysis at 1.6 V; (b) SEM and EDX of the cathode surfaces after test.

shown in Fig. 14(b), which may contribute to the decrease of the electro-catalytic activity of the cathodes.

4. Conclusion

In this work, Ni-loaded LSTO–SDC cathodes were used for steam electrolysis in an oxide-ion-conducting solid oxide electrolyzer with 3% H_2O/5% H_2/Ar and 3% H_2O/Ar fed to the cathodes at 800 °C. Significant improvements in electrochemical performance and current efficiency were achieved by loading a Ni catalyst onto the LSTO–SDC composite electrode for steam electrolysis with or without a flowing reducing gas over the cathodes. More importantly, the synergetic effect of catalytically-active Ni and redox-stable LSTO–SDC leads to the stability and the good performance of the composite cathode during direct steam electrolysis. However, the long-term performance of the composite cathode design is partly constrained by the agglomeration of the nickel particles under high-temperature operational conditions.

Appendix A. Supplementary data

Supplementary data related to this article can be found at http://dx.doi.org/10.1016/j.jpowsour.2013.06.107.

References

[1] J.D. Holladay, et al., Catal. Today 139 (2009) 244–260.
[2] R.M. Dell, D.A.J. Rand, R. Soc. Chem. (2008).
[3] S.P.S. Badwal, S. Giddey, C. Munnings, WIREs Energy Environ. (2012), http://dx.doi.org/10.1002/wene.50.
[4] V. Utgikar, T. Thiesen, Int. J. Hydrogen Energy 31 (2006) 939–944.
[5] J.S. Herring, J.E. O'Brien, C.M. Stoots, G.L. Hawkes, J.J. Hartvigsen, M. Shahnam, Int. J. Hydrogen Energy 32 (2007) 440–450.
[6] H. Uchida, N. Osada, M. Watanabe, Electrochem. Solid-State Lett. 7 (2004) A500–A502.
[7] A. Hauch, S.D. Ebbesen, S.H. Jensen, M. Mogensen, J. Mater. Chem. 18 (2008) 2331–2340.
[8] R.M. Xing, Y.R. Wang, S.H. Liu, C. Jin, J. Power Sources 208 (2012) 276–281.
[9] M.A. Laguna-Bercero, J.A. Kilner, S.J. Skinner, Solid State Ion. 192 (2011) 501–504.
[10] X.D. Yang, J.T.S. Irvine, J. Mater. Chem. 18 (2008) 2349–2354.
[11] T. Ishihara, N. Jirathiwathanakul, H. Zhong, Energy Environ. Sci. 3 (2010) 665–672.
[12] G. Tsekouras, J.T.S. Irvine, J. Mater. Chem. 21 (2011) 9367–9376.
[13] F. Bidrawn, G. Kim, G. Corre, J.T.S. Irvine, J.M. Vohs, R.J. Gorte, Electrochem. Solid-State Lett. 11 (2008) B167–B170.
[14] B. Yu, W.Q. Zhang, J. Chen, J.M. Xu, S.R. Wang, Sci. China Ser. B Chem. 51 (2008) 289–304.
[15] K.F. Chen, N. Ai, S.P. Jiang, Int. J. Hydrogen Energy 37 (2012) 10517–10525.
[16] K. Xie, Y.Q. Zhang, G.Y. Meng, J.T.S. Irvine, Energy Environ. Sci. 4 (2011) 2218–2222.
[17] D. Sarantaridis, A. Atkinson, Fuel Cells 7 (2007) 246–258.
[18] S.D. Ebbesen, M. Mogensen, J. Power Sources 193 (2009) 349–358.
[19] K. Haberko, M. Jasinski, P. Pasierb, M. Radecka, M. Rekas, J. Power Sources 195 (2010) 5527–5533.
[20] Y. Matsuzaki, I. Yasuda, Solid State Ion. 132 (2000) 261–269.
[21] S.D. Ebbesen, R. Knibbe, M. Mogensen, J. Electrochem. Soc. 159 (2012) F482–F489.
[22] S.W. Tao, J.T.S. Irvine, Nat. Mater. 2 (2003) 320–323.
[23] S.W. Tao, J.T.S. Irvine, S.M. Plint, J. Phys. Chem. B 110 (2006) 21771–21776.
[24] Y. Gan, J. Zhang, Y.X. Li, S.S. Li, K. Xie, J.T.S. Irvine, J. Electrochem. Soc. 159 (2012) F763–F767.
[25] S.S. Xu, S.S. Li, W.T. Yao, D.H. Dong, K. Xie, J. Power Sources 230 (2013) 115–121.
[26] X.B. Zhu, Z. Lu, B. Wei, M.L. Liu, X.Q. Huang, W.H. Su, Electrochim. Acta 55 (2010) 3932–3938.
[27] S.W. Tao, J.T.S. Irvine, Chem. Mater. 16 (2004) 4116–4121.
[28] S.S. Li, Y.X. Li, Y. Gan, K. Xie, G.Y. Meng, J. Power Sources 218 (2012) 244–249.
[29] J.H. Kim, D. Miller, H. Schlegl, D. McGrouther, J.T.S. Irvine, Chem. Mater. 23 (2011) 3841–3847.
[30] D. Neagu, J.T.S. Irvine, Chem. Mater. 22 (2010) 5042–5053.
[31] J.C. Ruiz-Morales, J. Canales-Vazquez, C. Savaniu, D. Marrero-Lopez, W.Z. Zhou, J.T.S. Irvine, Nature 439 (2006) 568–571.
[32] J. Canales-Vazquez, M.J. Smith, J.T.S. Irvine, W.Z. Zhou, Adv. Funct. Mater. 15 (2005) 1000–1008.
[33] X.G. Zhang, M. Robertson, C. Deces-Petit, W. Qu, O. Kesler, R. Maric, D. Ghosh, J. Power Sources 164 (2007) 668–677.
[34] S.P. Jiang, S. Zhang, Y.D. Zhen, W. Wang, J. Am. Ceram. Soc. 88 (2005) 1779–1785.
[35] Y.X. Li, J.E. Zhou, D.H. Dong, Y. Wang, J.Z. Jiang, H.F. Xiang, et al., Phys. Chem. Chem. Phys. 14 (2012) 15547–15553.
[36] M.J. Jorgensen, M. Mogensen, J. Electrochem. Soc. 148 (2001) A433–A442.